Studying the interaction of hydrophobically modified ethoxylated urethane (HEUR) polymers with sodium dodecylsulphate (SDS) in concentrated polymer solutions

Mervat S. Ibrahim[a,b], Jordane Valencony[a], Stephen King[c], Martin Murray[d], Agnieszka Szczygiel[d], Bruce D. Alexander[a], and Peter C. Griffiths[a,*]

[a] Faculty of Engineering and Science, University of Greenwich, Medway Campus, Chatham Maritime, Kent ME4 4TB, UK

[b] Pharmaceutics Department, Faculty of Pharmacy, Modern Science and Arts University,26 July Mehwar Road intersection with Wahat Road, Cairo, Egypt

[c] Science and Technology Facilities Council, ISIS Facility, Rutherford Appleton Laboratory, Didcot, Oxfordshire OX11 OQX, UK

[d] AkzoNobel, Wexham Road, Slough, Berkshire, SL2 5DS, UK

Telephone: +44(0) 208 331 9927

Email: p.griffiths@gre.ac.uk

Abstract

Hypothesis

Hydrophobically modified ethoxylated urethane polymers (HEURs) are widely used to control the rheological profile of formulated particulate dispersions through associative network formation, the properties of which are perturbed by the presence of surfactants. At high polymer concentrations and in the presence of surfactants, it is hypothesised that the dominant factors in determining the rheological profile are the number and composition of the mixed hydrophobic aggregates, these being defined by the number and distribution of the hydrophobic linkers along the polymer backbone, rather than the end-group hydrophobe characteristics *per se* that dominate the low polymer concentration behaviour.

Experiments

Three different HEUR polymers with formulae (C_6-L-(EO_{100}-L)$_9$-C_6, C_{10}-L-(EO_{200}-L)$_4$-C_{10} and C_{18}-L-(EO_{200}-L)$_7$-C_{18} (where L = urethane linker, C_n = hydrophobic end-group chain length, and EO = ethylene oxide block) have been studied in the absence and presence of SDS employing techniques that quantify (a) the bulk characteristics of the polymersurfactant blend, (b) the structure and composition of the hydrophobic domains, (c) the dynamics of the polymer and surfactant, and (d) the polymer conformation. Collectively, these experiments demonstrate how molecular-level interactions between the HEURs and sodium dodecylsulphate (SDS) define the macroscopic behaviour of the polymer/surfactant mixture.

Findings

Binding of the SDS to the polymer *via* two mechanisms - monomeric anti-cooperative and micellar cooperative - leads to surfactant-concentration-specific macroscopic changes in the viscosity. Binding of the surfactant to the polymer drives a conformational rearrangement, and an associated redistribution of the polymer end-groups and linker associations throughout the hydrophobic domains. The composition and size of these domains are sentisitve to the polymer architecture. Therefore, there is a complex balance between polymer molecular weight, ethylene oxide block size, and number of urethane linkers, coupled with the size of the hydrophobic end-groups. In particular, the urethane linkers are shown to play a hitherto largely neglected but important role in driving the polymer association.

Keywords: HEUR, SDS, viscosity, PGSE-NMR, surface tension, fluorescence, EPR, SANS, polymer/surfactant complex, telechelic polymers.

Introduction

Hydrophobically modified polymers (HMPs) are water-soluble polymers comprising hydrophilic backbones into which hydrophobic chains have been chemically incorporated, often classified as end-capped or comb-like depending on the location of these hydrophobic groups (1). Also known as associative thickeners, there are three common types: ethylene oxide-urethane block copolymers, hydrophobically-modified alkali-swellable (HASE) and a family of cellulose derivatives (2). This paper focuses on the first, *viz* hydrophobically modified ethylene oxide urethane block copolymers, or hydrophobically modified ethoxylated-urethane (HEUR) thickeners. HEURs are widely used to control the rheological profile of formulated particulate dispersions.

The presence of hydrophobic regions in the HMP structure induces a complex, concentration-dependent set of *inter*- and *intra*-molecular associations, dependent on factors such as the length of the hydrophilic backbone and the number, length, and distribution of the hydrophobic groups. Below the critical overlap concentration (C^*), end-capped HMPs adopt the so-called loop, bridge, closed loop conformations, as well as forming flower micelles. At concentrations above the overlap concentration, HMPs tend to associate into super-bridges, super-loops, dangling ends, and hence form networks of flower micelles (3–8). Most of the published papers in this area focus on the flower micelle forming HMPs.

Various techniques have been used to characterise the hydrophobic aggregates of model systems of hydrophobically modified PEO (PEOM), $C_nEO_mC_n$. The number of polymer end-groups (or polymer chains) aggregating per micelle (N_{agg}) can be detected using quenching fluorescence, electron-paramagnetic resonance (EPR) and small-angle neutron scattering (SANS) techniques. EPR has been used to determine the N_{agg} of $C_{12}EO_{200}C_{12}$ using 16-doxyl-stearic methyl ester (16-DSE) as a probe, the polymer N_{agg} is 31 ± 6. Microviscosity and effective relative permeability, which is correlated to the polarity of the polymer aggregates have been determined as well showing no change as a function of $C_{12}EO_{200}C_{12}$ concentration (9). Fluorescence experiments have been employed to determine the N_{agg} of PEOM $C_{16}EO_{100}C_{16}$. The CAC of $C_{16}EO_{100}C_{16}$ is 0.001 wt%. The polymer forms spherical

hydrophobic aggregates each consisting of 10 ± 1 chain loops. Over a wide range of concentration, N_{agg} 22 ± 2 per micelle, reflective of the insensitivity of the flower micelle size to concentration. Francois and co-workers found, using SANS and small-angle X-ray scattering (SAXS), that the core size of PEOM increases at very high concentrations (10,11). The scattering from the PEO in the flower micelle shows at least one broad peak at small Q value and a second one that appears as a shoulder at high-Q value. These peaks indicate a liquid-like order that is temperature and concentration dependent. These diffraction patterns are characteristic of a cubic phase (7,12).

The polymer arrangement changes as a function of polymer concentration. Bridges are formed between the flower micelles as the polymer concentration increases to form secondary aggregates, clusters, of a specific size (13). The mean number of bridge-forming chains per micelle increases linearly as a function of polymer concentration and a network structure is formed (13,14). The network structure has been studied as a function of shear by Richey *et al.* who synthesised a HEUR polymer with a pyrene group attached to the hydrophobic end group (15). The fluorescence was recorded throughout the shearing process. The intensity ratio remains constant as a function of shearing, though the rheology experiment shows a shear thinning behaviour. The invariant pyrene probe intensity confirms that the shear thinning behaviour is not accompanied by a change in the polymer micellar structures, and that the shear thinning behaviour is correlated to the breakage of the bridges connecting the hydrophobic aggregates.

The interaction between sodium dodecylsulphate (SDS) and HMPs affect some properties of the polymer system such as viscosity, self-diffusion coefficient, hydrophobicity, and size of the hydrophobic aggregates. In the HEUR and PEOM series of polymers, the SDS interacts with two sites in the polymer; the hydrophobic end-group, and the PEO backbone. The interaction of SDS with the hydrophobes forms polymer/SDS mixed hydrophobic aggregates, whereas a bead and necklace structure is formed as a result of SDS interaction with PEO, as well-documented in the literature (16–19).

The effect of SDS on the viscosity of HEUR solutions has been extensively reported previously; in general, the viscosity increases to a maximum at a characteristic SDS concentration before decreasing. The SDS concentration at which this maximum occurs shifts to a lower SDS concentration for polymers with a longer hydrophilic backbone or hydrophobic end groups (2,20,21). A similar behaviour has been observed for other HMPs (22–24).

The local structure has been probed by several techniques such as EPR to characterise the polarity of the hydrophobic aggregate of $C_{12}EO_{200}C_{12}$ with increasing SDS concentration (9) and diffusion NMR to measure the self-diffusion coefficient. The results demonstrate the formation of larger aggregates with increasing SDS concentration (25,26).

This study focuses on correlating the macroscopic and microscopic properties of SDS and HEUR systems using a range of techniques with particular focus on polymer concentrations well above the critical overlap concentration (C^*). Three polymers with different hydrophobic and EO chain lengths are explored to understand how the molecular structure of the polymer impacts on its interaction with SDS, thereby manifesting the bulk characteristics.

Materials and methods

Materials

Hydrophobically modified ethoxylated urethane (HEUR) polymers are generally synthesised in two steps: (a) reaction between poly(ethylene glycol) (PEG) and the urethane linker, 4,4'-diisocyanatodicyclohexylmethane (H_{12}MDI) is used for the polymers studied here, through step polymerization technique that yields an ethoxylated urethane pre-polymer and subsequently (b) reacting this prepolymer with alcohol to provide the hydrophobic end caps, Figure 1 (27,28).

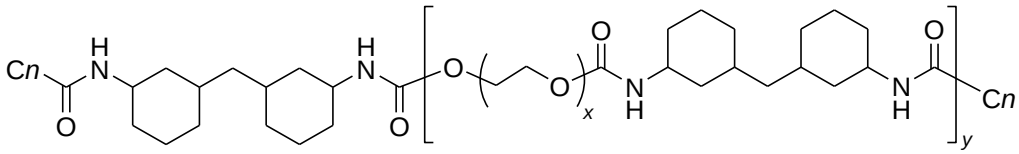

Figure 1. General structure of HEURs studied here, where Cn is the hydrophobic end-group, x number of EO unit, y number of polyurethane segments.

The samples employed here were all gifts from Dow, from their RM range. Here, we denote these polymers more schematically as C_n-L-$(EO_x$-L$)_y$-C_n where C_n denotes the length of the hydrophobic end group, L the urethane linker, x the number of ethylene oxide units per "block" , and y the number of blocks per polymer. Sodium dodecylsulphate (SDS) (Aldrich, no impurity observed), deuterated sodium dodecylsulphate (d_{25}-SDS) (ISIS deuteration facility), Hydroin buffer pH 9 (Aldrich), deionized water (18 MΩ cm, Purite Select deionizer) and deuterium oxide (Aldrich, purity 99.9%) were used as received.

Polymer	Hydrophobic end-group length, N	Number of ethylene oxide segments per block, x	Number of blocks per polymer, y
C_6-L-(EO_{100}-L)$_9$-C_6	6	100	9
C_{10}-L-(EO_{200}-L)$_4$-C_{10}	10	200	4
C_{18}-L-(EO_{200}-L)$_7$-C_{18}	18	200	7

Table 1. Structure of the HEUR polymers studied in this paper.

Methods

All samples were prepared in Hydroin buffer at pH 9 (pH checked by Orion Star A111 pH meter), the buffer ionic strength is 100 mM. All measurements were carried out at a temperature of 25 ± 0.5°C.

Rheology

Viscosity was recorded at 25 °C at a shear rate of 0.4 s^{-1} on a Malvern GEM 200 rheometer using a cone and plate geometry (4/40) calibrated against silicone oil. Sample volumes were 1.5 ml.

Pulsed-Gradient Spin-Echo Nuclear Magnetic Resonance (PGSE-NMR)

Polymers and surfactants were dissolved in Hydroin buffered deuterium oxide (D_2O), pH 9. Experiments were carried out at 25 °C on a 400 MHz Bruker FT NMR spectrometer. A stimulated echo sequence was used, in which the diffusion time (Δ) was set to 800 ms, the duration of the gradient pulses (δ) was held constant at 1 ms and their intensity (G) varied from 5 - 800 G cm^{-1}. Typically, 16 scans were accumulated over 32 gradient steps. Self-diffusion coefficients were extracted by fitting the peak intensities (I) to Equation 1 for the peaks at 3.75 ppm (EO) where I_0 is the signal intensity in the absence of gradient pulses, D_s the diffusion coefficient, γ the gyromagnetic ratio of protons (29,30).

$$I = I_0 \, e^{-D_s \gamma^2 G^2 \delta^2 \left(\Delta - \frac{\delta}{3}\right)} \qquad \text{Equation 1}$$

Surface tension

The surface tension of aqueous polymer/surfactant solutions was measured at 25 °C using a maximum bubble pressure tensiometer (SITA Science online t60), calibrated with deionized water. Samples were prepared in Hydroin buffered water, pH 9. A bubble lifetime of 10 seconds was used to ensure full equilibration.

Fluorescence

For all samples, a stock solution of 8-anilinonaphthalene-1-sulphonic acid (ANS) was first prepared in Hydroin buffered water (pH 9) at a concentration of 2.5 x 10^{-5} M. All samples were then prepared from this ANS stock solution and measured after 24 hours of preparation. Measurements were performed on Horiba Jobin Yvon Fluoromax-4 spectrophotometer at 25 °C in a semi-micro quartz cell. The excitation frequency was set to 380 nm, and the excitation spectrum recorded over wavelength range 400-600 nm (31).

Electron-paramagnetic Resonance (EPR)

EPR spectra of the water-insoluble spin-probe 16-doxyl-stearic acid methyl ester (16-DSE) solubilised into hydrophobic domains have been examined as a function of SDS and HEUR polymer concentrations. A range of SDS concentrations were mixed with the polymer at two concentrations, 7 wt% and 1 wt%. A concentration of 3 µg/ml of 16-DSE was used in all HEUR, SDS and blend samples. The probe samples were mixed for 24 hours in a hula-mixer before measurement.

EPR spectra were recorded at 25 °C on a CMS 8400 ADANI EPR spectrometer, centre field set to 337.4 mT, sweep width 6 mT, amplitude 70 uT, power attenuation 12 dB, gain value 1, gain order 3, sweep time 50 s. Each EPR spectrum is an average of four scans.

Neutron Scattering

SANS measurements were carried out at 25 °C on the SANS 2D instrument (ISIS spallation Neutron Source, Oxfordshire, UK). Neutrons wavelengths spanning 2-14 Å were used to access a Q range of 0.002 to 3 $Å^{-1}$ ($Q = 4\pi \sin(\theta/2)/\lambda$) (32) with a fixed sample-detector distance of 4 and 2.4 m for the rear and front detector, respectively. Temperature control was achieved through the use of a thermostatted circulating bath pumping fluids through the base of the sample changer, which allowed the experiment to be run at 25 ± 0.5 °C. Samples were contained in UV-spectrophotometer grade 1 mm path length quartz cuvettes (Hellma). The scattering data were normalized for the sample transmission and the incident

wavelength distribution, corrected for instrumental and sample backgrounds using a quartz cell filled with D_2O (this also removes the incoherent instrumental background arising from vacuum windows), and corrected for the linearity and efficiency of the detector response using the instrument specific software package. The data were put onto an absolute scale using a well characterised, partially deuterated polystyrene blend standard sample. The intensity of the scattered radiation, $I(Q)$, as a function of the wave vector, Q, is given by Equation 2:

$$I(Q) = N_p V_P^2 \Delta\rho^2 P(Q) S(Q) + B_{inc} \qquad \text{Equation 2}$$

where V_p is the volume of the scattering species, N_p the number of scattering species, $\Delta\rho$ the difference between the neutron scattering length density of the scattering species and the solvent, *P(Q)* describes the morphology of the scatstering species and, *S(Q)* describes the spatial arrangement of the scatterers in solution, B_{inc} incoherent background.

Results and discussion

The interaction of the anionic surfactant SDS has been studied with three HEURs, namely C_6-L-$(EO_{100}$-L$)_9$-C_6, C_{10}-L-$(EO_{200}$-L$)_4$-C_{10}, and C_{18}-L-$(EO_{200}$-L$)_7$-C_{18} at two polymer concentrations, $C_{polymer}$, spanning the critical overlap concentration (C^*) of C_6-L-$(EO_{100}$-L$)_9$-C_6 which is the key polymer investigated here, C^* = 3 wt%, *viz* $C_{polymer}$ = 1 wt% and $C_{polymer}$ = 7 wt%. For consistency, similar concentrations were used for the other two polymers. The concentrated systems are the subject of the main paper, whereas the dilute regime systems have been largely included in the supplemental as the conclusions from those studies are entirely consistent with literature precedence. Where appropriate, comparisons between the behaviour of the HEUR/SDS in the dilute and concentrated regimes will be made in the main paper.

The study is laid out thus - interaction of the polymer with surfactant results in changes in the bulk viscosity and polymer diffusion, therefore the polymer viscosity and self-diffusion coefficient are studied as a function of SDS. Changes in the structure and dynamics of the hydrophobic domains formed from the polymer hydrophobic end-groups and the surfactant have been studied by fluorescence and electron paramagnetic resonance (EPR). Finally, a

series of contrast match neutron scattering experiments are presented to study the arrangement of the polymer and surfactant in the polymer/surfactant blends.

Solution behaviour of HEUR/SDS mixtures

The viscosity and self-diffusion coefficient of C_6-L-(EO_{100}-L)$_9$-C_6 as a function of SDS concentration were measured above C^* and are presented in Figure 2 (a) and (b), respectively. The viscosity and self-diffusion data are generally complementary to each other; an increase in viscosity is reflected by a decrease in the self-diffusion coefficient. With increasing SDS concentration, the viscosity increases to a local maximum (V_{max}), then decreases, before it plateaus at higher SDS concentrations. The self-diffusion coefficient, therefore, follows a similar, inverted profile. Analogous observations are reported for C_{10}-L-(EO_{200}-L)$_4$-C_{10} and C_{18}-L-(EO_{200}-L)$_7$-C_{18}, Figure 2 (a) and (b). Before V_{max}, the polymer viscosity curve shows the trend C_{10}-L-(EO_{200}-L)$_4$-C_{10} < C_6-L-(EO_{100}-L)$_9$-C_6 < C_{18}-L-(EO_{200}-L)$_7$-C_{18}, which agrees with the polymer viscosity curves as a function of their concentration, Figure 3 (a). After V_{max}, the relative order of the viscosity curves slightly change, C_{18}-L-(EO_{200}-L)$_7$-C_{18} < C_{10}-L-(EO_{200}-L)$_4$-C_{10} and C_6-L-(EO_{100}-L)$_9$-C_6. In addition, the C_{18}-L-(EO_{200}-L)$_7$-C_{18} shows the greatest decrease in the viscosity.

Analogously, the diffusion data shows the highest diffusion below D_{min} for C_{10}-L-(EO_{200}-L)$_4$-C_{10} > C_6-L-(EO_{100}-L)$_9$-C_6 > C_{18}-L-(EO_{200}-L)$_7$-C_{18} (Figure 2 (b)), in agreement with the diffusion of simple polymers as a function of their concentration, Figure 3 (b). However, after D_{min}, the trends are again different where the highest diffusion is for C_{10}-L-(EO_{200}-L)$_4$-C_{10} > C_{18}-L-(EO_{200}-L)$_7$-C_{18} > C_6-L-(EO_{100}-L)$_9$-C_6. The D_{min} in the dilute regimes are shifted to lower SDS concentration for C_{18}-L-(EO_{200}-L)$_7$-C_{18} < C_{10}-L-(EO_{200}-L)$_4$-C_{10} < C_6-L-(EO_{100}-L)$_9$-C_6, Figure 2 (c and d).

a

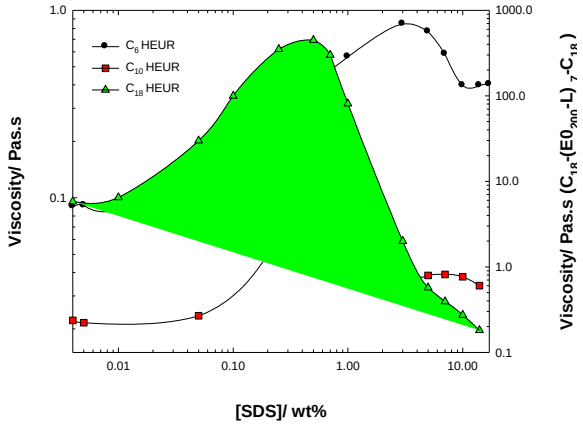

b

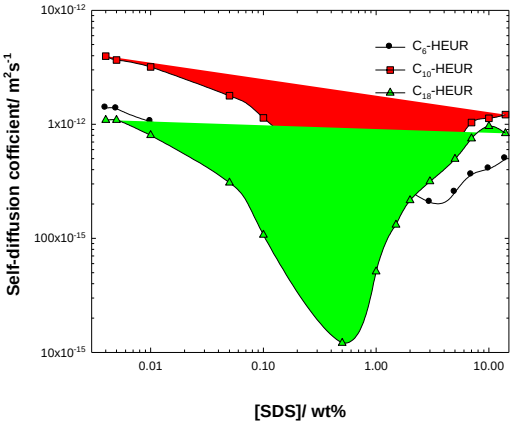

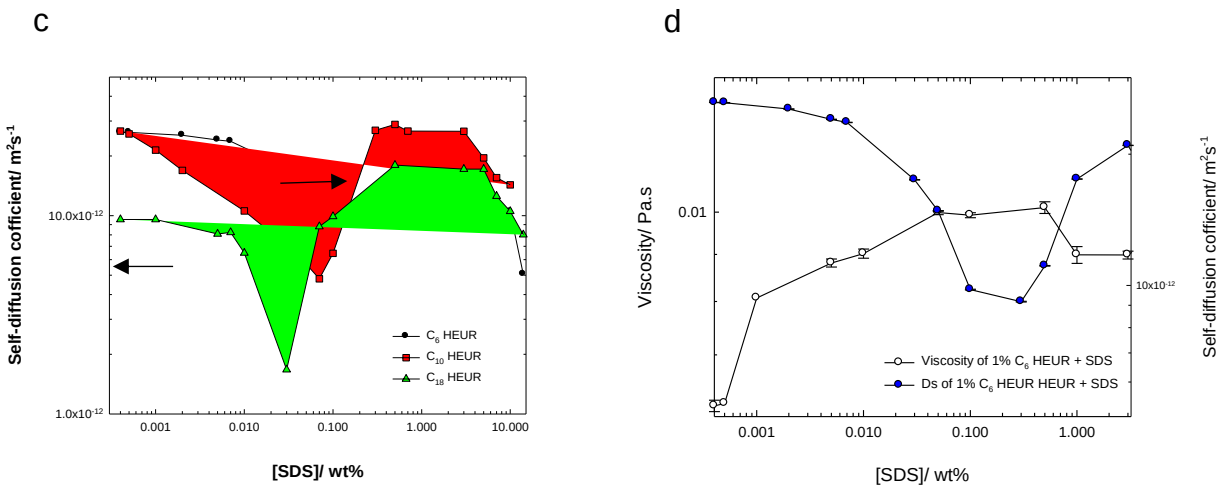

Figure 2. (a) viscosity at shear rate 0.1 s^{-1} and (b) self-diffusion coefficient of 7 wt% C_6-L-(EO_{100}-L)$_9$-C_6 (circles), C_{10}-L-(EO_{200}-L)$_4$-C_{10} (squares), and C_{18}-L-(EO_{200}-L)$_7$-C_{18} (triangles) as a function of SDS concentration, (c) viscosity (white circles) at shear rate 0.1 s^{-1} and self-diffusion coefficient (blue circles) of aqueous solutions of 1 wt% C_6-L-(EO_{100}-L)$_9$-C_6/SDS mixtures as a function of SDS concentration and (d) self-diffusion coefficient of 1 wt% C_6-L-(EO_{100}-L)$_9$-C_6 (circles), C_{10}-L-(EO_{200}-L)$_4$-C_{10} (squares), and C_{18}-L-(EO_{200}-L)$_7$-C_{18} (triangles) as a function of SDS concentration. Measurements were carried out at 25 °C, pH 9, and ionic strength 100 mM. The solid lines are guides for the eye.

Generally, the increase in viscosity (and decrease in self-diffusion coefficient) with increasing surfactant concentration reflects the number and composition of mixed micelles of SDS and hydrophobic end-groups, as this defines the strength of the polymer network. The network is generally strengthened by increasing the residence time of the polymeric end-groups within such micelles or increasing the number of cross-links by increasing the number of hydrophobic aggregates, or conversion of loop-forming polymer chains to bridges (1,2).

At 7 wt% HEUR, a dense network conformation is expected where most of the loop-forming polymer chains in the polymer hydrophobic aggregates are converted to bridges. Therefore the adoption of a different conformation for the polymer chains as a function of SDS is excluded. The viscosity increase (and diffusion decrease) can be correlated with the strengthening of the network structure due to the formation of more aggregates of smaller size, therefore, the number of cross-links increase, hence the viscosity increases. At higher SDS concentration, the polymer hydrophobes are solubilised in SDS micelles which annul

their presence. As a result, the network structure is broken and the HEUR behaves in a similar manner to PEO/SDS mixtures (15,26).

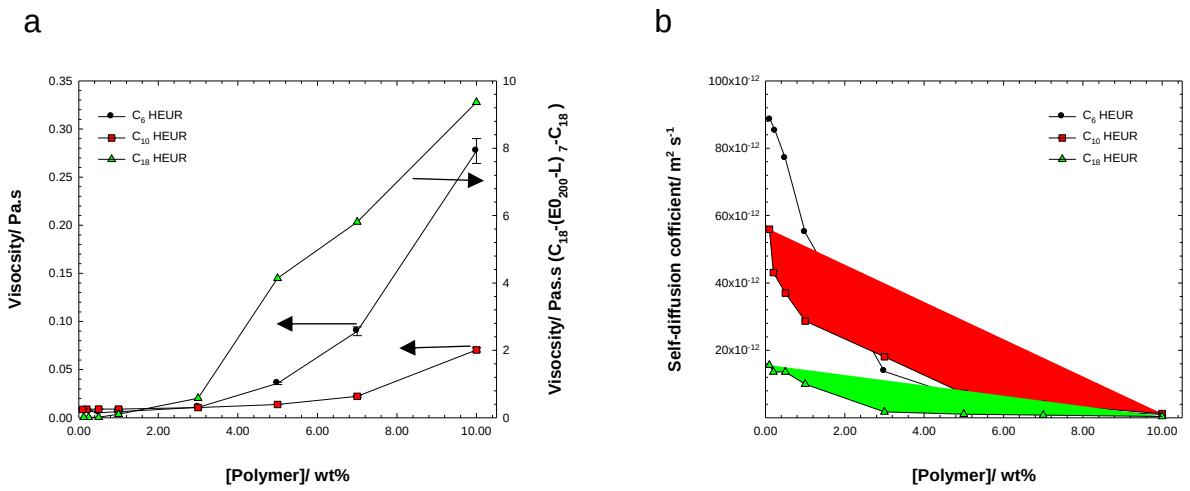

Figure 3. (a) viscosity (b) self-diffusion cofficient of C_6-L-(EO_{100}-L)$_9$-C_6 (circles), C_{10}-L-(EO_{200}-L)$_4$-C_{10} (squares), and C_{18}-L-(EO_{200}-L)$_7$-C_{18} (triangles) at shear rate 0.1 s^{-1} as a function of polymer concentration. Measurements were carried out at 25 °C, pH 9, and ionic strength 100 mM. The solid lines are guides for the eye.

Analysis of HEUR/SDS hydrophobic aggregates

Since the diffusion/viscosity insights reflect different, but complementary facets of the polymer/surfactant blend, fluorescence was also used to probe the effect of SDS on the hydrophobic domains, formed initially from the polymer end-groups, Figure 4 (a). In the ANS fluorescence experiment, variation in the structure and composition of the hydrophobic domain leads to changes in the measured ANS intensity as the fluorescence yield is sensitive to the interaction between the two organic rings in the ANS molecule, a factor that is sensitive to both the polarity and fluidity of the probe location. This technique is a useful experimental approach to probe for anionic surfactant micellization, showing a substantial increase in the measured intensity at the CMC, Figure S.4, with the fluorescence estimate for the CMC = 0.05 wt% showing excellent agreement with the same value extracted from the surface tension data (0.06 wt%, Figure S.1).

The fluorescence data for C_6-L-(EO_{100}-L)$_9$-C_6 as a function of SDS concentration show a decrease of ANS intensity to a minimum (I_{min}), which then slightly rises at higher SDS concentration, Figure 4 (a). I_{ANS} decreases with reduced ANS solubilisation, or the environment is less polar and/or one that is more mobile. A combination of all of these factors is likely to be occurring here. The ANS intensity of C_{18}-L-(EO_{200}-L)$_7$-C_{18} was not measured as the viscosity of the sample was too high in presence of SDS. There are very subtle

differences between the ANS intensity of the C_6-L-(EO_{100}-L)$_9$-C_6 and C_{10}-L-(EO_{200}-L)$_4$-C_{10}, Figure 4 (a). In the concentrated regime, the decrease in the ANS intensity is likely due to the formation of smaller aggregates of HEUR/SDS mixed micelles (as will be shown latter in the scattering data) as well as the binding of the charged SDS monomers and the associated counter-ion to the hydrophobic aggregates increasing the polarity of the thus-formed mixed micelle. The increase in I_{ANS} at higher SDS concentrations is due to the cooperative micellar binding of SDS micelles. The gross features of the ANS intensity curves below C^* are similar to the polymer behaviour in the concentrated regime, however, the I_{min} is shifted to lower SDS concentrations, Figure 4 (b). The decrease in the I_{ANS} in the dilute regime is correlated to the changes in the polarity of the mixed micelles, as the scattering data doesn't show any evidence of significant change in aggregate size.

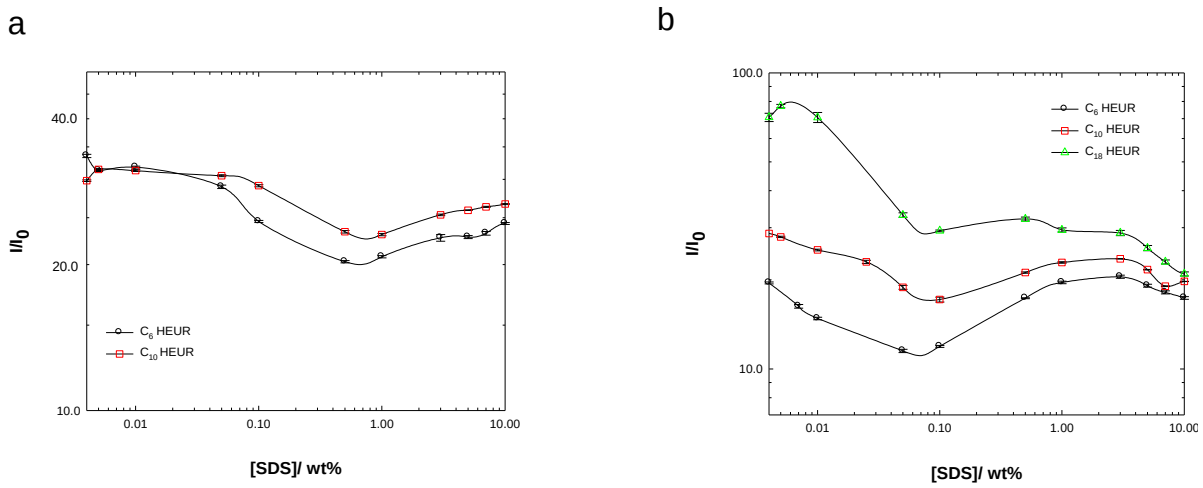

Figure 4. ANS fluorescence of (a) 7 wt% C_6-L-(EO_{100}-L)$_9$-C_6 (circles), C_{10}-L-(EO_{200}-L)$_4$-C_{10} (squares) and (b) 1 wt% C_6-L-(EO_{100}-L)$_9$-C_6 (circles), C_{10}-L-(EO_{200}-L)$_4$-C_{10} (squares), C_{18}-L-(EO_{200}-L)$_7$-C_{18} (triangles) as a function of SDS concentration. Measurements were carried out at 25 °C, pH 9, and ionic strength 100 mM. The ANS intensity of C_{18}-L-(EO_{200}-L)$_7$-C_{18} has not been measured due to very high viscosity. The solid lines are guides for the eye.

The change in the hydrophobic aggregate structure as the SDS interacts with the polymer is also reflected by changes in 16-DSE signal measured by electron paramagnetic resonance (EPR). The 16-DSE shows a signal for 7 wt% C_6-L-(EO_{100}-L)$_9$-C_6 for all the SDS concentrations used in this study (0.1, 1, and 3 wt%) indicative of the presence of hydrophobic aggregates, Figure 5, left column. The EPR spectrum shows splitting of the 1st (low-field) and 3rd (high-field) peak for all polymer/surfactant blends. The peak splitting is reflective of the presence of two different environments, which we ascribe to polymer-like and surfactant-like environments by comparison with the reference single component

systems. A similar behaviour is observed for the C_{18}-L-$(EO_{200}$-L$)_7$-C_{18} (Figure 5, right column) but not for the C_{10}-L-$(EO_{200}$-L$)_4$-C_{10}. For the C_{10}-L-$(EO_{200}$-L$)_4$-C_{10} case (Figure S.5), left column), the data are much noisier, indicative of the absence of polymer dominated hydrophobic domains of sufficient size to solubilise the probe. It is interesting that this corresponds to the polymer system with the fewest urethane linkers, suggesting that the urethane groups are key component to the aggregation. When SDS is present in the system, the observed behaviour for C_{10}-L-$(EO_{200}$-L$)_4$-C_{10} is dominated by the SDS-rich environment, however, for the C_{18}-L-$(EO_{200}$-L$)_7$-C_{18} the two environments are observed at the higher SDS concentrations.

These observations are quite distinct to those made from model systems. Persson *et al.* studied the polarity of $C_{12}EO_{200}C_{12}$/SDS in dilute systems by EPR using 16-DSE. The polarity sensed by the probe increases as the SDS interacts with the PEO end-group hydrophobes up to 20-30 mM (7). The polarity decreased at higher SDS concentration due to the increase in the N_{agg} of SDS. Those results agree with the fluorescence data (Figure 4 (b)), however the ANS I_{min} is observed at lower SDS concentration 1 mM (0.05 wt%) and intensity increased at 17 mM (0.5 wt%) to reach the value of C_6-L-$(EO_{100}$-L$)_9$-C_6 in the absence of SDS. The increase in the ANS intensity after I_{min} is interpreted differently here, where it is hypothesised that the increase in the intensity is due to the cooperative micellar binding of SDS micelles, rather than changes in the SDS N_{agg}. The scattering data presented in Figure 6 and Figure S.7 suggests the absence of change in the size of the SDS micelles adsorbed to the polymer as a function of SDS concentration where I_{ANS} increases after I_{min}, hence no change in SDS N_{agg} may occur.

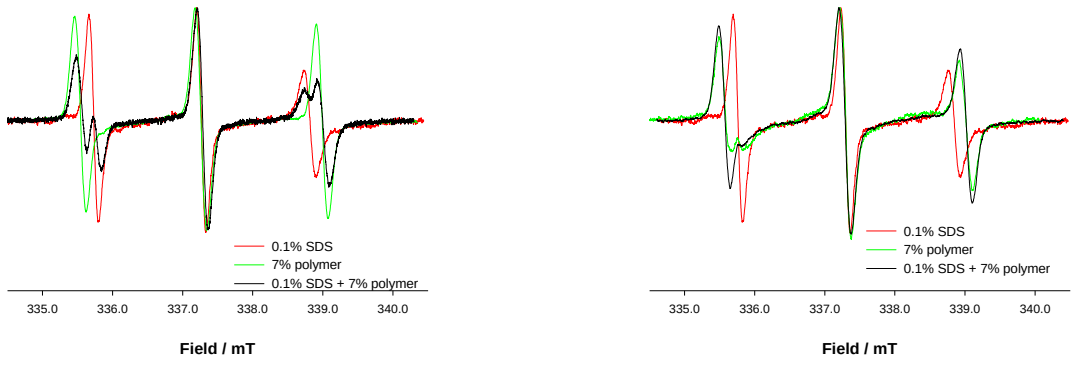

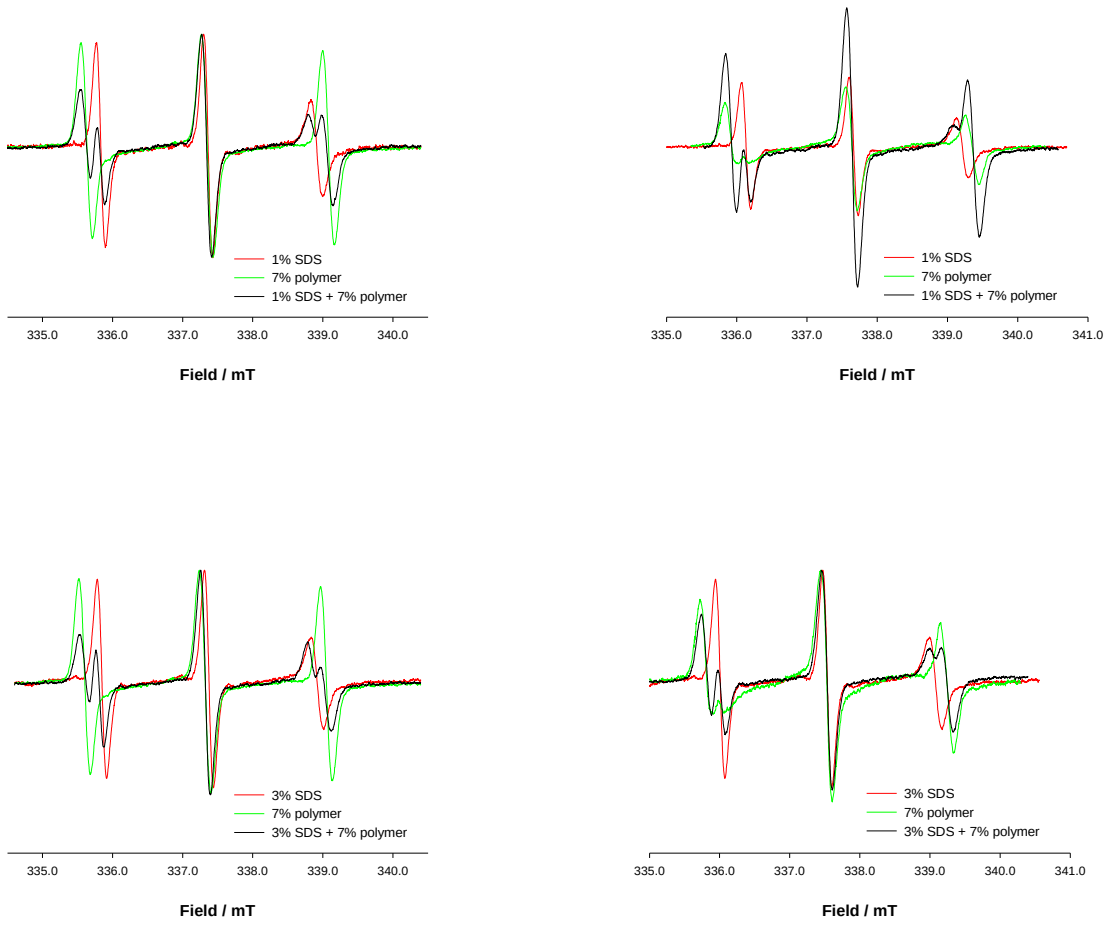

Figure 5. EPR spectrum for 16-DSE in presence of three different concentrations of SDS, and a fixed polymer concentration of 7 wt%; C_6-L-(EO_{100}-L)$_9$-C_6 (left panel) and C_{18}-L-(EO_{200}-L)$_7$-C_{18} (right panel), and the polymer/SDS blend. Measurements were carried out at 25 °C, pH 9, and ionic strength 100 mM.

As in the concentrated regime, the EPR data for C_6-L-(EO_{100}-L)$_9$-C_6 and C_{18}-L-(EO_{200}-L)$_7$-C_{18} below C^* in the presence of SDS also show two environments, Figure 5S.6 left and right columns respectively. The spectra from blends of C_{10}-L-(EO_{200}-L)$_4$-C_{10}/SDS at $C_{polymer}$ = 1 wt% are dominated by the SDS-rich environment, similar to the behaviour noted for the concentrated regime, Figure S.5, right column.

SANS from HEUR/SDS mixtures

To gain a better understanding of the polymer conformation, and the impact of the surfactant aggregation on the polymer conformation, a series of “contrast variation” neutron scattering

experiments were undertaken. The degree of interaction between the neutrons and a molecule consisting of atoms, *I*, is given by the scattering length density ρ, Equation 3:

$$\rho = \sum_i b_i \left(\frac{\delta N_A}{M_W}\right) \qquad \text{Equation 3}$$

where *b* is the scattering length, δ the bulk density, N_A Avogadro's number (6.02 x 10^{23} mol^{-1}), and M_W the molecular weight of the scattering body. The contrast is the difference in ρ value between the molecule of interest ρ_p, and the surrounding medium ρ_m, squared *i.e.* $(\Delta\rho)^2$ so if this equals zero there is little/no scattering and the scattering bodies are said to be "contrast matched". In such an approach, the scattering from the polymer or surfactant may be highlighted through judicious choice of hydrogenous and deuterated materials *e.g.* the scattering arising from a deuterated surfactant/hydrogenous polymer/hydrogenous solvent blend is dominated by the surfactant, whereas that from a deuterated surfactant/hydrogenous polymer/deuterated solvent blend arises principally from the polymer. The examination of the polymer/SDS systems with different contrasts has therefore be used to highlight different facets of the system.

First consider the overall scattering of the h-C_6-L-(EO_{100}-L)$_9$-C_6/h-SDS/D_2O,where the overall size and shape of the polymer/surfactant complex is characterised. There is an SDS concentration-dependent increase in intensity observed at mid-Q, Figure 6 (a), top row. The peak at mid-Q is shifted to higher-Q range as the SDS concentration increases. Worthy of note, is the presence of surfactant-like scattering around mid-Q (0.03 $Å^{-1}$) even at very low concentrations of SDS (this feature might be more aptly described as a shoulder but the term "peak" will be used to highlight the comparison with surfactant scattering), reflecting the structure of the aggregates of hydrophobic groups present within the polymer. The polymer peak emerges from a shoulder to a micelle-like scattering peak as the SDS concentration increases. This may be correlated to the decrease of the average size of the aggregates and hence smaller d-spacing is observed. Similar conclusions may be drawn from the overall scattering of the other two polymers, Figure 6 (b) and 6 (c), top row. In the dilute regime, similar observations are reported for the scattering curves at mid-Q, however at low-Q there is a concomitant decrease in intensity, indicative of repulsive interactions between charged structures Figure S.7, top row.

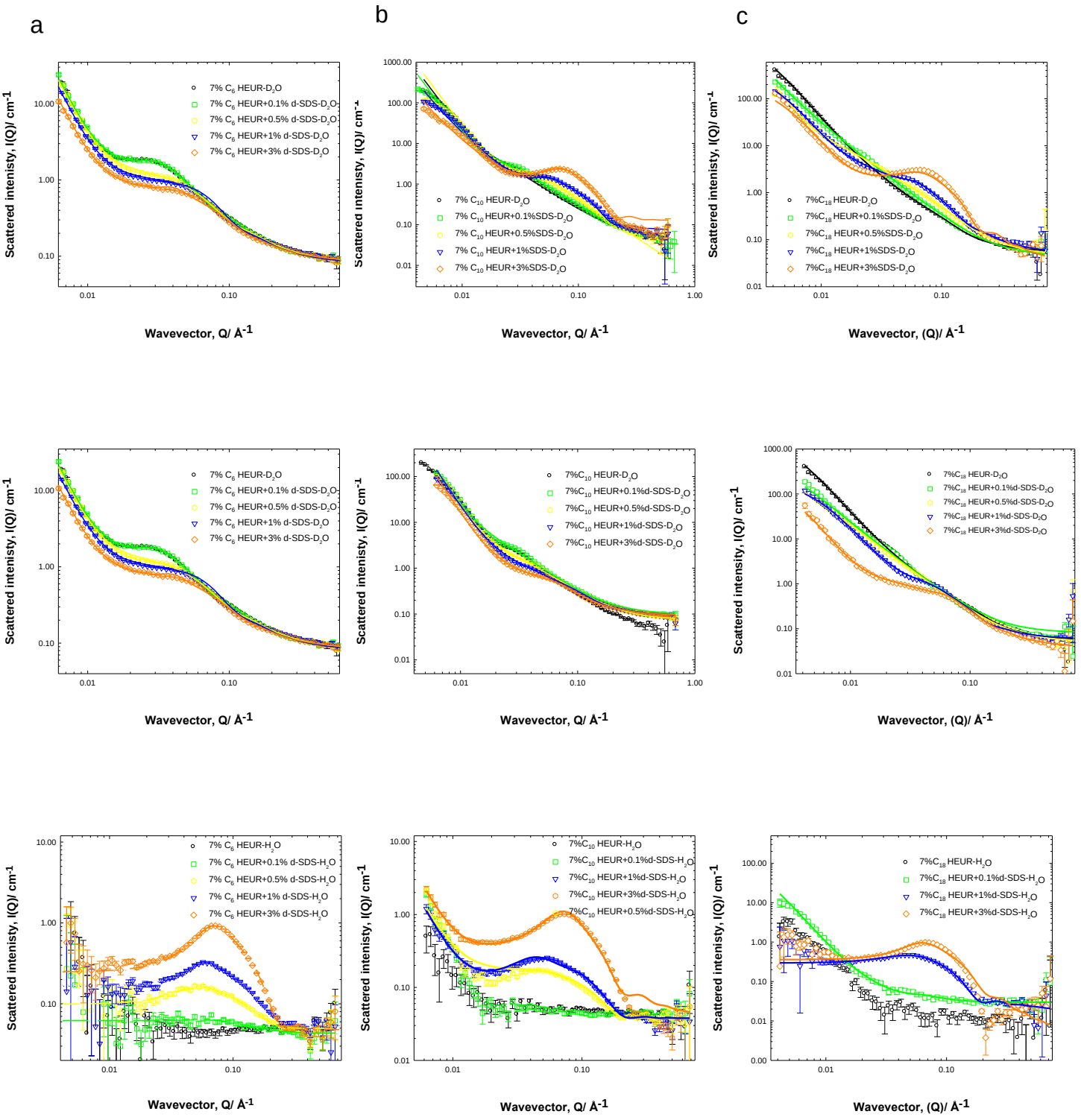

Figure 6. Comparison of Small-angle neutron scattering from the three polymers where column (a) shows the different contrasts for C_6-L-(EO_{100}-L)$_9$-C_6, (b) C_{10}-L-(EO_{200}-L)$_4$-C_{10}, and (c) C_{18}-L-(EO_{200}-L)$_7$-C_{18}. The three different contrast are h-polymer/h-surfactant/D_2O (top row), h-polymer/d-surfactant/D_2O (middle rowl), and h-polymer/d-surfactant/H_2O (bottom row); $C_{polymer}$ = 7 wt% with SDS 0 (circles), 0.1 (squares), 0.5 (hexagons), 1 (triangles) and 3 (diamonds) wt% 'last three points have been omitted for clarity'. Measurements were carried out at 25 °C, pH 9, and ionic strength 100 mM. The solid lines are fits for sphere and gel model.

In the h-C_6-L-(EO_{100}-L)$_9$-C_6/d-SDS/D_2O contrast, the intensity of the peak at mid-Q decreases as a function of SDS and moves to higher Q, Figure 6 (a), middle row. The changes in the C_6-L-(EO_{100}-L)$_9$-C_6 scattered intensity at low-Q is very subtle as a function of SDS concentration. The decrease in the scattered intensity of the polymer peak as a function of SDS concentrations indicates the decrease in the number of polymer hydrophobes in the mixed aggregates. The shift of the peak position to lower-Q reflects changes in the size and composition of the HEUR/SDS mixed aggregates, where smaller aggregates are formed, hence the d-spacing decreases. The subtle changes in the scattering at low-Q suggests the presence of insignificant changes in the conformation and hence the network structure, this agrees with the viscosity and diffusion data, over this range of SDS concentrations. Similar observations and conclusion may be drawn from the C_{10}-L-(EO_{200}-L)$_4$-C_{10}, Figure 6 (b), middle row. However, for C_{18}-L-(EO_{200}-L)$_7$-C_{18} (Figure 6 (c), middle row) the changes in the scattered intensity of the polymer backbone shows more significant decrease at 3 wt% SDS, indicative of the presence of polymer conformation changes in agreement with the viscosity data for this polymer, Figure 2 (a). In the dilute regime, the peak (0.02 $Å^{-1}$) in the 1 wt% HEUR disappears at low values of surfactant concentration, 0.1 and 0.5 wt% SDS, reflecting the conversion of polymer loops into bridges. The peak (0.02 $Å^{-1}$) reappears at higher SDS concentration, 1 and 3 wt%, where micellar binding of SDS to the PEO backbone occurs, the PEO starts to wrap itself around the SDS micelle as expected forming the bead-and-necklace model of PEO/SDS interaction, Figures S.7 (a), (b), and (c), middle row.

In the h-C_6-L-(EO_{100}-L)$_9$-C_6/d-SDS/H_2O contrast, the 0.1 wt% SDS shows a flat curve as the mixed aggregates are dominated by polymer hydrophobes, Figure 6 (a), bottom panel. The intensity of the peak increases as a function of SDS as the mixed micelles become more dominated by SDS. Similar conclusions may be drawn for the SDS scattering contrast of the other two polymers, Figures 6 (b), (c), bottom row. Worth mentioning, the SLD of the C_{10}-L-(EO_{200}-L)$_4$-C_{10} and C_{18}-L-(EO_{200}-L)$_7$-C_{18} was not perfectly matched and hence there is some minor scattering from the polymer at low-Q. Below C^*, there is a move towards more polymer-like scattering emerging in the surfactant-only scattering contrast, Figures S.7 (a), (b), and (c),bottom row. It is envisaged that the surfactant interacts first with the hydrophobic domains, illustrative of the micellar-like scattering, and then subsequently interacts with the polymer backbone, giving rise to the polymer-like form to the data in the scattering of SDS only.

Similar systems for pure PEOM and HEUR have been fitted to a polydisperse sphere model (11,12). However, this model does not capture the features of the data presented here, especially the low-Q data points. The steepness of the scattering curve at low-Q suggests the presence of large structures which can be correlated to the sparse network structure postulated by Suzuki *et al.* for telechelic polymers below C^* due to the connection of flower micelles *via* bridging polymer chains (33). Therefore, terms that describe network structure have been added to the model to capture all the features in these scattering curves. Saffer *et al.* used a two correlation length network model to describe two-phase net-like mesh structures formed by cross-linked PEG gels (34), these systems are very close to the system used here. Therefore, the scattering has been modeled using a compound model, comprising a solid sphere model to reflect the micelle scattering and a two correlation length model to reflect the polymeric network described by Equation 4:

$$\frac{\partial\sigma}{\partial\Omega}(Q) = N_p V_p^2 (\Delta\rho)^2 . \left(\left(\frac{4}{3}\pi R^3 \frac{[sin(QR) - QRcos(QR)]}{(QR)^3} * S(q) \right) + \frac{I_1}{(1+Q^2\xi^2)} + \frac{I_2}{(1+Q^2A^2)^2} \right) + B_{inc}$$

Equation 4

where N_p is the number of scattering species V_p the volume of scatterers, $\Delta\rho$ the difference of scattering length density between molecules and solvent, R the radius of the sphere, Q the wavevector, $S(q)$ sphere structure factor, I_1 the intensity of Lorentzian term of length ξ, I_2 the intensity of the Debye-Bueche term of length A, and B_{inc} the inchoherent background.

The sphere term will capture the radius of the hydrophobic HEUR aggregates, SDS micelle, or HEUR/SDS mixed aggregates. The structure factor of the sphere is represented by the charge density (C) per SDS micelle or the HEUR/SDS mixed micelle and inversely the Debye screening length. Two correlation lengths are considered which may describe a shorter length scale $'\xi'$ which defines the mesh size of the network and a longer length scale 'A' which may be correlated to the distance between the inhomogenous centres of the system. However, the correlation length values extracted from the fit for the polymers studied here suggested that the shorter length scale may describe gel network structure fluctuation, whereas the longer length scale is approaching the limit of the instrument resolution *e.g.* an extended polymer network.

In the dense network regime, the size of the aggregates decrease as the SDS concentration increases, where a shift from a large polymer aggregate to a SDS micelle sized aggregate is observed. The fit is sensitive to the micelle charge at higher SDS concentrations only, 1

and 3 wt%. The length scales of the polymer show very subtle changes as a function of SDS concentration, Table 2. Similar conclusions may be drawn from the other two polymers, fits are presented in the supplemental section, Tables S.1 and S.2. The sphere structure factor at low SDS concentrations can be “turned off”, however, at higher SDS concentration (1 and 3 wt%) the fit becomes sensitive to the charge.

In the polymer scattering contrast in the concentrated regime, the parameters are in good agreement with those extracted from the overall scattering contrast, Table 3, S.6 and S.7. In the C_{18}-L-(EO_{200}-L)$_7$-C_{18} at 1 and 3 wt% SDS, the network structure is broken, reflected by decrease in the scattered intensity at low-Q and decrease in the ξ and A length scales. The decrease in the polymer length scales at 1 wt% and 3 wt% can be explained by a collapse of the polymer chains as the latter wraps itself around the SDS micelles.

Unsurprisingly, the surfactant-only contrast show aggregates with size consistent with an SDS micelle for all the SDS concentrations, Table 4, S.11 and S.12.

In the dense network regime, the only change observed is related to the aggregate size and composition, at least over the range of SDS concentration studied here. The decrease of the sphere radius is reflective of the formation of smaller polymer hydrophobic aggregates. There is a less significant change in the polymer length scale which may be correlated to the maintaining of the polymer network structure in the SDS range studied in this experiment. This agrees with the viscosity data where the decrease in viscosity, which is correlated to the breakage of the network structure, is observed at SDS concentrations higher than 3 wt%. However, in the dilute regime the size of the aggregates measured in presence of SDS is equal to the SDS micelle size. In addition, changes in the polymer conformation evidenced by changes in the polymer scattered intensity at low-Q.

Below C^* and analogous to the concentrated regime, the length scales extracted from the polymer scattering contrast (Table S.8-S.10) and sphere size extracted from the surfactant scattering contrast (Table S.13-15) agree with the values of the same quantities extracted from the fit to the overall scattering contrast (Table S.3-S.5) . The only key difference is that the intensity of the shorter length scale is lower in the polymer-only contrast. Further, in the surfactant scattering contrast, the values for the shorter length scale support the hypothesis of the decoration by SDS monomers of the urethane linkers distributed along the polymer backbone.

Fit parameters/ Units	7 % HEUR + 0 % SDS	7 % HEUR + 0.1 % SDS	7 % HEUR + 0.5 % SDS	7 % HEUR + 1 % SDS	7 % HEUR + 3 % SDS
Intensity of radius term	1.8×10^{-6}	2.8×10^{-6}	6.5×10^{-6}	2.0×10^{-6}	7.5×10^{-5}
Radius (Å)	62 ± 5	52 ± 3	42 ± 3	35 ± 1	20
C	n.d.	n.d.	n.d.	10	10
I_1	1.7	1.4	1.4	0.8	0.9
ξ (Å)	20 ± 1	20 ± 1	16 ± 1	17 ± 1	14 ± 1
I_2	7190	7190	7190	6190	6000
A (Å)	672 ± 10	672 ± 10	672 ± 10	672 ± 10	672 ± 10

Table 2. SANS key parameters from the sphere and network model for C_6-L-(EO_{100}-L)$_9$-C_6 /SDS/D_2O at $C_{polymer}$ = 7 wt%.

Fit parameters/ Units	7 % HEUR + 0 % SDS	7 % HEUR + 0.1 % SDS	7 % HEUR + 0.5 % SDS	7 % HEUR + 1 % SDS	7 % HEUR + 3 % SDS
Intensity of radius term	1.8×10^{-6}	2.0×10^{-6}	2.0×10^{-6}	2.2×10^{-6}	1.9×10^{-6}
Radius (Å)	62 ± 5	54 ± 3	42 ± 3	35 ± 1	30 ± 1
C	n.d.	n.d.	n.d.	10	10
I_1	1.7	1.2	0.8	0.7	0.7
ξ (Å)	20 ± 1	20 ± 1	17 ± 1	17 ± 1	17 ± 1
I_2	7190	7190	7190	5490	3400
A (Å)	672 ± 10	670 ± 10	674 ± 10	674 ± 10	674 ± 10

Table 3. SANS key parameters from the sphere and network model for C_6-L-(EO_{100}-L)$_9$-C_6 /d-SDS/D_2O $C_{polymer}$ = 7 wt%.

Fit parameters/ Units	7 % HEUR + 0.5 % SDS	7 % HEUR + 1 % SDS	7 % HEUR + 3 % SDS
Intensity of radius term	4.0×10^{-6}	5.5×10^{-6}	4.8×10^{-5}
Radius (Å)	18	20	17
C	n.d.	10	10
I_1	0.065	0.03	0.002
ξ (Å)	7	4	3
I_2	n.d.	n.d.	n.d.
A (Å)	n.d.	n.d.	n.d.

Table 4. SANS key parameters from the sphere and network model for C_6-L-(EO_{100}-L)$_9$-C_6 /d-SDS/H_2O $C_{polymer}$ = 7 wt%.

Compare the viscosity, fluorescence and EPR data for the two similarly sized polymers C_6-L-(EO_{100}-L)$_9$-C_6 and C_{10}-L-(EO_{200}-L)$_4$-C_{10} - the viscosity at 7 wt% for C_6-L-(EO_{100}-L)$_9$-C_6 > C_{10}-L-(EO_{200}-L)$_4$-$C_{10;}$ fluorescence data illustrate the increased partitioning of ANS in the C_{10}-L-(EO_{200}-L)$_4$-C_{10} case relative to C_6-L-(EO_{100}-L)$_9$-C_6 ; whilst the EPR data shows no signal (and therefore partitioning of 16-DSE) for the C_{10}-L-(EO_{200}-L)$_4$-$C_{10,}$ whereas the C_6-L-(EO_{100}-L)$_9$-C_6 has a signal from the 16-DSE reflective of the presence of hydrophobic aggregates of sufficient size capable of solubilising that probe. Therefore, an indirect conclusion may be drawn that C_6-L-(EO_{100}-L)$_9$-C_6 seems to have a stronger association through the urethane linkers (viscosity, EPR) but the C_{10}-L-(EO_{200}-L)$_4$-C_{10} has an increased number of- but smaller hydrophobic aggregates (ANS).

As an aside, the importance of the urethane linkers in promoting the association of the polymer has been studied by SANS. The ability of β-cyclodextrin to form complexes with the HEUR hydrophobic end-groups has been previously reported by Liao *et al.* (37,38). Here, β-cyclodextrin was added to the polymer solution to form a 1:1 end-group - β-cyclodextrin complex at 5 wt% C_6-L-(EO_{100}-L)$_9$-C_6 and the scattering from the polymer recorded, and contrasted with the same in the absence of the β-cyclodextrin. Intriguingly, the intensity of

the shoulder at 0.03 $Å^{-1}$ arising due to polymer self-association decreased in the presence of β-cyclodextrin, but does not disappear, Figure 7**Error! Reference source not found.Error! Reference source not found.**. Thus, it may be concluded that association of the polymer occurs significantly through the urethane linkers, as this interaction cannot be nullified by the cyclodextrin.

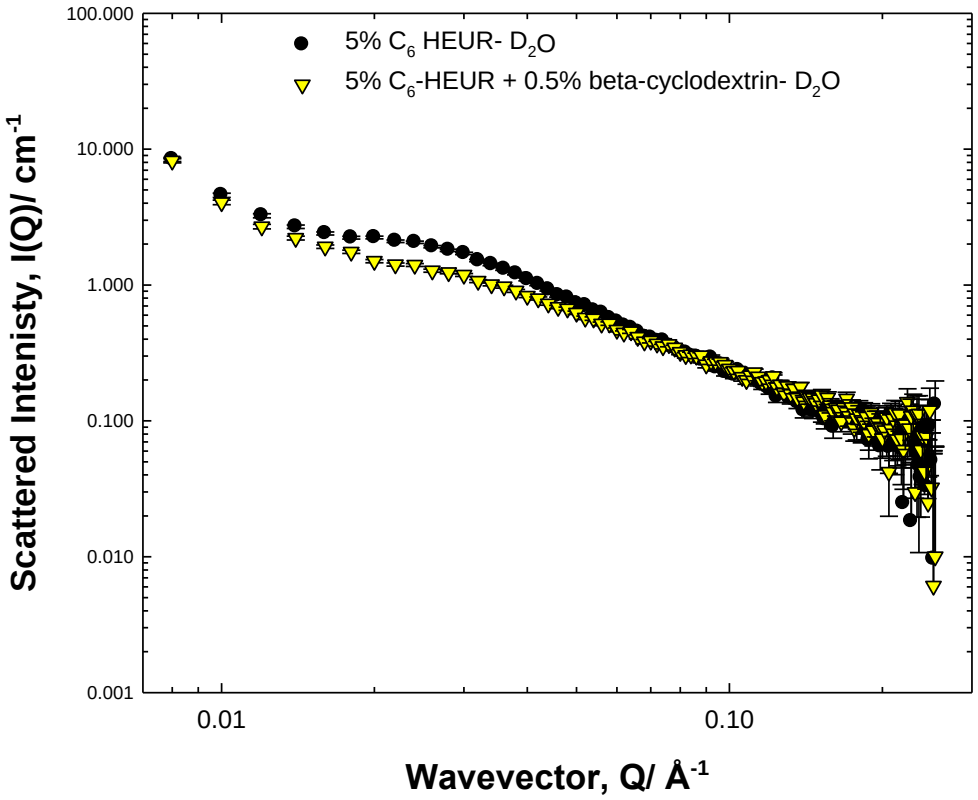

Figure 7. Small-angle neutron scattering from 5 wt% C_6-L-(EO_{100}-L)$_9$-C_6 in absence (circles) and presence (triangles) of 0.5 wt% β-cyclodextrin.

Conclusions

HEUR polymers and surfactants are present in many formulations *e.g.* paints and cosmetics, often at much higher concentrations than those studied in the literature. Understanding the behaviour of the HEUR in the presence of surfactants is important for optimizing these formulations. In this paper, concentrated solutions of three polymers with general structure C_n-L-(EO_x-L)$_y$-C_n have been studied as a function of SDS concentration. It is very clear in this study, that there is a much stronger correlation of the observed behaviour with the urethane linker content - the polymers that possess more linkers show higher viscosity

(slower diffusion) in comparison with those with fewer linkers. The viscosity, diffusion data together with the scattering of the polymer in presence of β-cyclodextrin, which annulled the polymer association through the hydrophobic end-groups, suggest the presence of polymer association through the urethane linkers.

There is evidence of a strong interaction between the urethane linkers and the SDS, an interaction often neglected in published work. Characterisation of the dilute solution behaviour of these systems reproduced trends reported in literature (1–3), but it is further shown that there is a more structure sensitive behaviour in these systems at higher polymer concentrations.

Comparing the SANS experiments on dilute and concentrated regime highlights rather different behaviour for the three polymers. In the dilute regime sparse network structure is formed where the flower micelles are the building unit of the network, therefore the changes observed in the various techniques used are due to loss of this arrangement. Above C^* there are fewer flower micelles and a dense network is observed. These significant changes may be interpreted in terms of the number and composition of the mixed polymer hydrophobe / surfactant micelles rather than the polymer conformation per se.

Since this study highlighted the importance of urethane linkers in the association and interaction with SDS, more clear cut conclusions could be drawn by fixing the molecular weight of the polymer and the length of the hydrophobic end-group and only the urethane linkers number shall be varied.

References

1. Karlson L. Hydrophobically modified polymers rheology and molecular associations. Ph.D. Thesis, *University of Lund*. **2002**.

2. Huldun, M. Hydrophobically modified urethane-ethoxylate (HEUR) associative thickeners 1. Rheology of aqueous solutions and interactions with surfactants. *Colloids Surfaces A Physicochem*. **1994**;*82*:263–277.

3. Annable T, Buscall R, Ettelaie R, Whittlestone D. The rheology of solutions of associating polymers : Comparison of experimental behavior with transient network theory. *J Rheol.* **1992**;*37*:695-726.

4. Annable T, Buscall R, Ettelaie R. Network formation and its consequences for the physical behaviour of associating polymers in solution. *Colloids Surfaces A Physicochem Eng Asp.* **1996**;*11*:97-116.

5. Paeng KW, Kim B, Kim E, Sohn D. Aggregation processes of hydrophobically modified polethylene oxide. *Bull Korean Chem Soc*. **2000**; *21*: 623-627.

6. Yekta A, Xu B, Duhamel J, Adiwidjaja H, Winnik MA. Fluorescence studies of associating polymers in water-determination of the chain-end aggregation number and a model for the association process. *Macromolecules*. **1995**;*28*(4):956–966.

7. Gourier C, Beaudoin E, Duval M, Sarazin D, Maitre S, Francois J. A light scattering study of the association of hydrophobically alpha- and alpha, omega-end-capped poly(ethylene oxide) in water. *J Colloid Interface Sci*. **2000**;*230*(1):41–52.

8. Lafleche F, Durand D, Nicolai T. Association of adhesive spheres formed by hydrophobically end-capped PEO. 1. Influence of the presence of single end-capped PEO. *Macromolecules*. **2003**;*36*(4):1331–1340.

9. Persson K, Bales BL. EPR study of an associative polymer in solution: determination of aggregation number and interactions with surfactants. *J Chem Soc Faraday Trans*. **1995**;*91*(17):2863-2870.

10. Abrahmsen-Alami S, Alami E, Francois J. The lyotropic cubic phase of model associative polymers : Small-angle X-Ray scattering (SAXS), differential scanning calorimetry (DSC), and turbidity measurements. *J Colloid Interface Sci*.

2000;*179*(179):20–33.

11. Francois J, Maitre S, Rawiso M, Sarazin D, Beinert G, Isel F. Neutron and X-ray scattering studies of model hydrophobically end-capped poly(ethylene oxide) aqueous solutions at rest and under shear. *Colloids Surfaces A Physicochem Eng Asp*. **1996**;*112*(1-2):251-265.

12. Beaudoin E, Lapp A, Hiorns RC, Grassl B, François J. Neutron scattering of hydrophobically modified poly(ethylene oxide) in aqueous solutions in the presence of latex particles. *Polymer*. **2002**;*43*(9):2677–2689.

13. Raspaud E, Lairez D, Adam M, Carton JP. Triblock copolymers in a selective solvent. 1. Aggregation process in dilute solution. *Macromolecules*. **1994**;*27*(11):2956–2964.

14. Xu B, Yekta A, Li L, Masoumi Z, Winnik MA. The functionality of associative polymer networks: The association behavior of hydrophobically modified urethane-ethoxylate (HEUR) associative polymers in aqueous solution. *Colloids Surfaces A Physicochem Eng Asp*. **1996**;*112*(2-3):239–250.

15. Richey B, Kirk AB, Eisenhart EK, Fitzwater S, Hook J. Interactions of associative thickeners with paint components as studied by the use of a fluorescently labeled model thickener. *J Coatings Technology*. **1991**;*63*(798):31–40.

16. Brown W, Fundin J, Graca Miguel M. Poly(ethylene oxide)-sodium dodecyl sulfate interactions studied using static and dynamic light scattering. *Macromolecules*. **1992**;*25*(26):7192–7198.

17. Smitter LM, Guedez JF, Muller AJ, Saez AE. Interactions between poly(ethylene oxide) and sodium dodecyl sulfate in elongational flows. *J Colloid Interface Sci*. **2001**;*236*(2):343–353.

18. Jones MN. The interaction of sodium dodecyl sulfate with polyethylene oxide. *J Colloid Interface Sci*. **1967**;*23*(1):36–42.

19. Francois J, Dayantis J, Sabbadin J. Hydrodynamical behaviour of the poly(ethylene oxide) -sodium dodecylsulphate complex. *Eur Polym J*. **1985**;*21*(2):165–174.

20. Kaczmarski JP, Glass JE. Synthesis and solution properties of hydrophobically-modified ethoxylated urethanes with variable oxyethylene spacer lengthst. *Macromolecules*. **1993**;*26*(19):5149–5156.

21. Lundberg DJ, Brown RG, Glass JE, Eley RR. Synthesis, characterization, and solution rheology of model hydrophobically-modified, water-soluble ethoxylated urethanes. *Langmuir*. **1994**;*10*(9):3027–3034.

22. Regalado EJJ, Vallejo CCR, Textle HM, Guerrero R, Munoz JFE. Influence of hydrophobe, surfactant and salt concentrations in hydrophobically modified alkali-soluble polymers obtained by solution polymerization. *J Mex Chem Soc*. **2012**;*56*(2):1387-1396.

23. Volpert E, Selb J, Candau F. Associating behaviour of polyacrylamides hydrophobically modified with dihexylacrylamide. *Polyme*r. **1998**;*39*(5):1025–1033.

24. Thuresson K, So O, Hansson P, Wang G. Binding of SDS to ethyl(hydroxyethyl)cellulose. Effect of hydrophobic modification of the polymer. *J Phys Chem.* **1996**:*100*(12):4909–4918.

25. Alami E, Almgren M, Brown W. Interaction of hydrophobically end-capped poly(ethylene oxide) with nonionic surfactants in aqueous solution. Fluorescence and light scattering studies. *Macromolecules*. **1996**;*29*(14):5026–5035.

26. Persson K, Griffiths PC, Stilbs P. Self-diffusion coefficient distributions in solutions containing hydrophobically modified water-soluble polymers and surfactants. *Polymer*. **1996**;*37*(2):253–261.

27. Najafi F, Pishvaei M. Synthesis and characterization of nonionic urethane based linker. *Prog Color Color Coat*. **2011**;*4*:71–77.

28. Barmar M, Barikani M, Kaffashi B. Synthesis of ethoxylated urethane and modification with cetyl alcohol as thickener. *Iran Polym J*. **2001**;*10*(5):331–335.

29. Abrahmsen-Alami S, Stilbs P. NMR self-diffusion of associative polymers in aqueous solution : The influence of the hydrocarbon end-chain length on the polymer transport dynamics in single- and two-component mixtures. *J Colloid Interface Sci*. **1997**;*189*(1):137–143.

30. Claridge. High-Resolution NMR Techniques in Organic Chemistry. Second. Oxford,UK: ELSVIERE; **2009**.

31. Hawe A, Sutter M, Jiskoot W. Extrinsic fluorescent dyes as tools for protein characterization. *Pharm Res*. **2008**;*25*(7):1487–1499.

32. Heenan RK, King SM, Turner DS, Treadgold JR. SANS2d at the ISIS second target station. 17th Meet Int Collab Adv Neutron Sources. 2005;1–6. Available from: http://www.isis.stfc.ac.uk/instruments/sans2d/publications/sans2d-at-isis10323.pdf, (acessed January 2017).

33. Suzuki S, Uneyama T, Watanabe H. Concentration dependence of nonlinear rheological properties of hydrophobically modified ethoxylated urethane aqueous solutions. *Macromolecules*. **2013;***46*(9):3497–3504.

34. Saffer EM, Lackey MA, Griffin DM, Kishore S, Tew GN, Bhatia SR. SANS study of highly resilient poly(ethylene glycol) hydrogels. *Soft Matter*. **2014**;*10*(12):1905-1916.

35. Rosen M. Surfactants and interfacial phenomena. Second edition. New York, *Wiley*: USA; **1989**.

36. Dai S, Tam KC, Wyn-Jones E, Jenkins RD. Isothermal titration calorimetric and electromotive force studies on binding interactions of hydrophobic ethoxylated urethane and sodium dodecyl sulfate of different molecular masses. *J Phys Chem B*. **2004**;*108*(16):4979–4988.

37. Liao D, Dai S, Tam KC. Rheological properties of hydrophobic ethoxylated urethane (HEUR) in the presence of methylated β-cyclodextrin. *Polymer*. **2004**;*45*(25):8339–48.

38. Liao DS, Dai S, Tam KC. Influence of anionic surfactant on the rheological properties of hydrophobically modified polyethylene-oxide/cyclodextrin inclusion complexes. *J Rheol*. **2009**;*53*(2):293–308.

39. Dai S, Tam KC, Wyn-Jones E, Jenkins RD. Isothermal titration calorimetric and electromotive force studies on binding interactions of hydrophobic ethoxylated urethane and sodium dodecyl sulfate of different molecular masses. *J Phys Chem B*. **2004**;*108*(16):4979–4988.